

*Supporting Information for*

# **Cysteine-Protected Antibacterial Spheroids of Atomically Precise Copper Clusters for Direct and Affordable Arsenic Detection from Drinking Water**

*Jenifer Shantha Kumar<sup>†‡</sup>, Arijit Jana<sup>†</sup>, Jayathraa Raman<sup>†‡</sup>, Hema Madhuri Veera<sup>†‡</sup>,  
Amoghavarsha Ramachandra Kini<sup>†</sup>, Jayoti Roy<sup>†</sup>, Saurav Kanti Jana<sup>†</sup>, Tiju Thomas<sup>‡</sup>, and  
Thalappil Pradeep<sup>†\*</sup>*

<sup>†</sup>Department of Chemistry, DST Unit of Nanoscience (DST UNS) and Thematic Unit of Excellence (TUE), Indian Institute of Technology Madras, Chennai 600036, India.

\*E-mail: [pradeep@iitm.ac.in](mailto:pradeep@iitm.ac.in)

<sup>‡</sup>Department of Metallurgical and Materials Engineering, Indian Institute of Technology Madras, Chennai 600036, India

This supporting information is a 26 page document, including the table of contents, 5 sections of experimental descriptions, 2 sections of discussions, 17 figures, 1 table and this cover page.

## Table of contents

Items	Description	Page No.
Text S1	Synthesis of Cu <sub>18</sub> NCs	3
Text S2	Synthesis of Cu <sub>17</sub> NCs	3
Text S3	Sensing experiments	3
Text S4	Antibacterial activity	3
Text S5	Analytical methods	4
Text S6	Characterization of Cu <sub>17</sub> NCs	7
Text S7	Increased affordability of the <i>As</i> sensor	8
Figure S1	Mass spectrum of Cu <sub>18</sub> NCs	9
Figure S2	Mass spectra of Cu <sub>16</sub> and Cu <sub>17</sub> NCs	10
Figure S3	TGA and DTA analysis of CASs	10
Figure S4	PL spectra of Cu <sub>17</sub> NCs in solution and coating	11
Figure S5	Linearity plot of arsenic detection	11
Table S1	Comparison of the Cu <sub>17</sub> NCs-based sensor's performance	12
Figure S6	XPS survey spectrum of Cu <sub>17</sub> NCs and selected spectra in the S 2p and O 1s regions	14
Figure S7	FTIR analysis of Cu <sub>17</sub> NCs	15
Figure S8	PXRD analysis of Cu <sub>17</sub> NCs	16
Figure S9	DLS analysis of Cu <sub>17</sub> NCs	17
Figure S10	PL plot of AIE enhancement	17
Figure S11	Selectivity towards arsenic	18
Figure S12	Selectivity towards arsenic in tap water	19
Figure S13	Effect of organic and inorganic arsenic	20
Figure S14	Antibacterial effect of CASs	21
Figure S15	ESEM images of <i>Staphylococcus aureus</i>	22
Figure S16	ESEM images of <i>Bacillus subtilis</i>	22
Figure S17	Electrochemical impedance spectroscopy of CASs	23
References		23

**Text S1. Synthesis of Cu<sub>18</sub> Nanoclusters.** Cu<sub>18</sub> Nanoclusters (NCs) were prepared according to the method reported by Li *et al.*<sup>1</sup> The CuI precursor (95 mg, 0.49 mM) was mixed with 0.03 mM (120 mg) of 1,2-bis-(diphenylphosphino) ethane (DPPE) under an argon environment. 15 ml of acetonitrile was added to it. After 30 min of stirring, the resulting mixture formed a white dispersion, which was reduced using 187 mg (320 mM) of dry NaBH<sub>4</sub>. The reaction was allowed to be continuously stirred at 600 rpm for 5 h. An orange-colored precipitate was formed, which was washed several times with acetonitrile and methanol. The extracted orange residue was dissolved in 4 ml dichloromethane (DCM) for further synthesis. UV-Vis and Electrospray ionization mass spectrometry (ESI MS) studies confirmed the formation of Cu<sub>18</sub>NCs with a relative yield of 70-75% in terms of Cu precursors.

**Text S2. Synthesis of Cu<sub>17</sub> NCs.** Here, 4 ml of purified Cu<sub>18</sub>NCs in DCM from S1 was taken in a fresh glass bottle, and 50 mg of L-cysteine (L-Cys) dissolved in methanol (2 ml) was added slowly in an inert condition to the Cu<sub>18</sub> NCs. The reaction was allowed to proceed for 2.5 h at 22 °C with 400 rpm stirring. Cluster-assembled-superstructures (CASs) were formed rapidly by mixing (DCM) and methanol solvents (1:1, v/v). The CASs were washed several times with methanol to remove excess reagents.

**Test S3. Sensing experiments.** The purified Cu<sub>17</sub>NCs of equal volume were used to drop cast on non-woven polypropylene (PP) discs (1 cm diameter) to observe the solid-state emission. Arsenite ( $As^{3+}$ ) and arsenate ( $As^{5+}$ ) solutions of various concentrations were prepared separately from their sodium salts in MilliQ water, and the pH was adjusted to 7.5. The interfering metal ion solutions were prepared similarly with CdCl<sub>2</sub>, HgCl<sub>2</sub>, FeCl<sub>3</sub>, PbCl<sub>2</sub>, CuCl<sub>2</sub> and CrCl<sub>3</sub> dissolved in water, and the pH was adjusted to 7. Sodium phosphate was used to prepare the phosphate solutions of various concentrations. The contaminated water was allowed to interact with PP discs for 10 minutes.

**Test S4. Antibacterial activity.** The antibacterial activity of Cu<sub>17</sub>NCs was studied against gram-negative bacteria *E. coli* (MTCC 443) and *E. coli* (MTCC 739) and gram-positive bacteria *B. subtilis* (ATCC 21331) and *S. aureus* (MTCC 740). The stock cultures of the bacteria were revived in fresh Luria Bertani (LB) Broth. Freshly cultured bacteria were grown from the revived culture in LB Broth to a cell density of  $\sim 10^8$  CFU/ml, and the O.D.<sub>600</sub> values were used to check the growth. The bacteria were diluted to  $\sim 10^2$  CFU/ml and drop-casted on sterile PP discs of 1 cm diameter and allowed to interact for 1 h. Following this, PP discs were inverted on the nutrient agar (NA) surface to transfer the bacterial cells from them. Similarly, this was done with sterilized PP discs coated with CuI/solvent (methanol and DCM in 1:1 ratio)/L-Cys/CASs. In short, the bacterial cells were allowed to interact with the coated PP discs for 1 hour and transferred onto freshly prepared NA plates through inversion. The NA plates were then incubated at 37 °C for 24 hours to allow the live cells to grow into colonies. The plate colony counting method was adapted to determine the number of viable cells. The experiments were carried out similarly for *E. coli* (MTCC 443), *E. coli* (MTCC 739), and gram-positive bacteria *B. subtilis* (ATCC 21331) to understand their effect on the bacterial cells. All the experiments were performed in triplicates.

Further, the antibacterial effect was investigated through Environmental Scanning Electron Microscopy (ESEM) imaging. The bacteria were drop cast on the cluster-coated PP discs. The bacterial cells were carefully collected from the discs by washing them with PBS. The collected cells were dehydrated through a graded ethanol treatment (20, 40, 60, 80, 95, 100% ethanol in water) for 10 minutes of exposure in each concentration. The dehydrated cells were subject to gold-sputtering and imaging. The antibiofilm property was investigated by allowing *B. subtilis* cells to grow on the cluster-coated silicon for three days at 37 °C. The grown cells from the sheets were collected with gentle washing and drop cast on stubs for ESEM imaging.

## **Text S5. Analytical methods**

### **UV-vis spectroscopy**

A PerkinElmer Lambda 365 spectrometer was utilized to record absorption spectra in the cluster solutions within the 200-800 nm wavelength range, employing standard quartz cuvettes with a 1 cm optical width.

### **Mass spectrometry**

ESI MS measurements of the parent NCs and ligand-exchanged products were analyzed by a Waters Synapt G2Si high-definition mass spectrometer. The instrument is equipped with an ESI source, step wave ion transfer cell, and quadrupole mass filter. The instrument's ion mobility cell was kept off during the studies. All measurements were recorded in the positive ion mode, and the following optimized parameters were employed during analysis: capillary voltage – 2.75 kV, sampling cone – 0 V, source offset – 0 V, source temperature – 100 °C, desolvation temperature – 150 °C. In addition, the desolvation gas flow was – 400 L/h, the nebulizer gas flow was 2.5 bar, and the ion energy was – 0.2.

### **Dynamic Light Scattering**

Dynamic Light Scattering (DLS) analysis was conducted using a Malvern Zetasizer ZSP device featuring a 633 nm (He-Ne) laser source.

### **Photoluminescence study**

The Horiba Jobin Yvon Nanolog was utilized to measure the photoluminescence (PL) spectra. All emission spectra were corrected and expressed in relative photon flux units to account for the wavelength-dependent response of the spectrometer and detector.

### **X-ray photoelectron spectroscopy**

The X-ray photoelectron spectroscopy (XPS) was carried out in the Omicron ESCA probe TPD instrument. Aluminium source was used to generate non-monochromatic X-rays from a dual anode source with an X-ray power of 300 W. The survey scan was done from 0 to 1100 eV with a pass energy of 50 eV and a step size of 0.5 eV to identify all the elements present in the sample. Detailed scans were done for all the elements of interest with a pass energy of 20 eV and a step size of 0.1 eV to get better resolution for the peaks.

### **Infrared spectroscopy**

The Perkin Elmer Fourier-transform infrared (FTIR) spectrometer was employed for sample measurements. 2.0 mg of NCs were mixed with 20 mg of dry potassium bromide to prepare the pellet.

### **Powder X-ray diffraction**

Powder X-ray diffraction (PXRD) measurements were conducted using a D8 Advance instrument manufactured by Bruker. A Cu K $\alpha$  X-ray source with an energy of 8047.8 eV was utilized. For all PXRD measurements, the sample was drop-cast onto a glass slide, resembling a thin film.

### **FESEM imaging**

The field emission scanning electron microscopy (FESEM) measurements of the CASs were carried out using a FEI Quanta FESEM operated in high vacuum mode with an operating voltage of 30 kV. The same instrument was used to record Energy-dispersive spectroscopy (EDS) spectra and perform elemental imaging.

## **ESEM imaging**

The bacterial samples were analyzed in ESEM under extended low vacuum mode using a FEI QUANTA-200 SEM. The voltage of the electron gun was set at 10 kV for the imaging.

## **TGA/DTA measurements**

Thermogravimetric analysis (TGA) and Differential thermal analysis (DTA) of about 3.5 mg of cluster sample in an alumina crucible were performed using a NETZSCH STA 449 F3 Jupiter instrument equipped with the Proteus-6.1.0 software. Both the measurements were performed under a nitrogen atmosphere at a flow rate of 20 ml/min in the temperature range of 30 to 700 °C with a heating rate of 10 °C/min.

## **Surface charge measurement**

The surface charge of the cluster film was measured by electrochemical impedance spectroscopy (EIS). With this aim, the freshly prepared CASs were coated on a glassy carbon electrode (GCE) and allowed to dry at room temperature. This was used as a working electrode, Pt was the counter electrode, and Ag/AgCl was the reference electrode during the EIS measurement. EIS was carried out using Biologic instrument (SP200) at a frequency of 1kHz. During measurement, a DC potential was varied between -1.2 to 0.8 V. We carried out all measurements at 1 kHz of an input AC signal (20 mV), and the DC potential applied to the cluster-coated film was varied from -1 to +0.8 V. Cluster film was coated on GCE. The GCE was appropriately cleaned with aluminium slurry prior to the cluster coating on it. For control, we performed EIS using bare and cluster-coated GCE in 0.5 M of NaCl.

**Text S6. Characterization of Cu<sub>17</sub>NCs.** The synthesis of Cu<sub>17</sub> and Cu<sub>18</sub>NCs was confirmed by UV-vis spectroscopy (Figure 1b) and mass spectrometry. The UV-vis spectra of both NCs show an increase in intensity from 250 nm to 360 nm, originating from the d→sp transition in CuNCs.<sup>1,2</sup> L-Cys does not show any absorption features in the UV-vis spectra.<sup>3</sup> Photographs of

as-synthesized Cu<sub>18</sub> and Cu<sub>17</sub>NCs are presented in the inset of Figure 1b, showing that the color of the solution changes from red to orange (Inset of Figure 1b) as the Ligand exchange induced structural transformation (LEIST) reaction proceeds (Figure 1a). Molecular composition of the clusters was investigated using high-resolution ESI MS studies. ESI MS spectrum of the precursor Cu<sub>18</sub>NCs shows a peak at m/z 1775 corresponding to the [Cu<sub>18</sub>(DPPE)<sub>6</sub>H<sub>16</sub>]<sup>2+</sup> form (Figure 1c), while the singly charged peak at m/z 3550 was also present in the spectrum (shown in Figure S1). The inset of Figure S1 shows that the mass spectra match well with the simulated spectra. The ESI MS spectrum agreed well with the previous reports.<sup>1,4</sup> Cu<sub>17</sub>NCs show an intense peak at m/z 3064.27 with a monpositive charge state, showing the composition of the clusters to be [Cu<sub>17</sub>S(L-Cys)<sub>3</sub>(DPPE)<sub>4</sub>]<sup>+</sup> (Figure 1c). The inset shows that the spectrum matches with the simulated one. Other compositions present in the system are [Cu<sub>16</sub>(DPPE)<sub>4</sub>(L-Cys)<sub>3</sub>H<sub>2</sub>]<sup>+</sup> (m/z 2972.5), originating from the loss of 1 Cu atom and [Cu<sub>17</sub>DPPE<sub>6</sub>(L-Cys)<sub>5</sub>]<sup>+</sup> (m/z 2020) with S loss (Figure S2). These have been matched to the corresponding theoretical mass spectra. TGA and DTA were performed on Cu<sub>17</sub>NCs in the solid state. There were no observed mass losses up to 150 °C (Figure S3). The first 6% loss in mass at 153 °C could be attributed to the loss of DPPE, while the subsequent mass loss at 192 °C is due to the loss of L-Cys and DPPE ligands. This shows that the Cu<sub>17</sub>NCs possess superior thermal stability in the solid state.

**Text S7. Increased affordability of the As sensor.** The sensing discs have been developed using CuNCs, which are much more affordable than their nanoparticle counterparts and common noble metal (Au, Ag) NCs.<sup>5-7</sup> As mentioned in the earlier literature, a sensor composed of non-noble metal-based NCs can reduce the cost per test several times.<sup>8,9</sup> Thus, it is evident that one of the primary reasons for the increased affordability of our system is the use of copper and the corresponding raw materials. Arsenic detection through Cu<sub>17</sub>NCs can be performed without preconcentration, additional reagents, and sample processing, which

enables rapid measurements. The PP mat-based sensing discs are easy to carry and are stable at room temperature. PP discs were chosen as the substrate for sensing films over a Whatman filter paper and printing paper as they did not absorb water quickly, allowing ions to interact effectively with the Cu<sub>17</sub>NCs coating.

From a practical perspective, the amount of Cu<sub>17</sub>NCs in each sensing disc is approximately 950 ng. The Cu<sub>17</sub>NCs were synthesized at room temperature and with less energy consumption than traditional synthetic processes, reducing production costs. With the cost of the reagents, PP mat, and other consumables for performing the test, the price of the materials per test is estimated to be \$0.01.

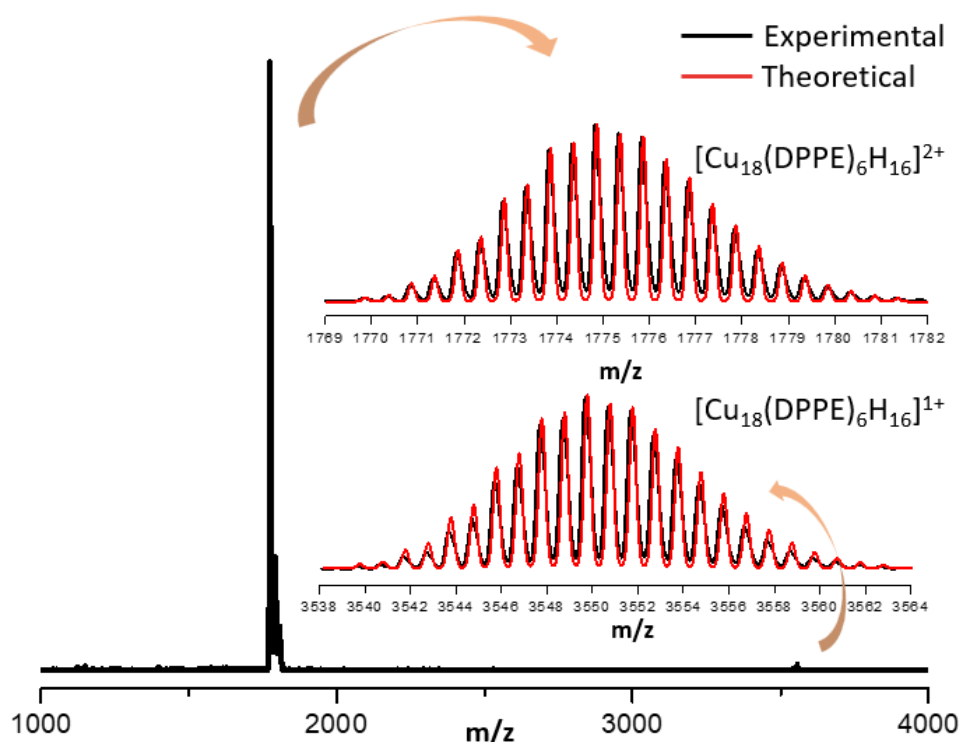


**Figure S1.** Full range ESI MS spectrum of Cu<sub>18</sub>NCs. The inset presents the expanded theoretical MS spectra matched with the recorded MS spectra of the doubly (top) and singly (bottom) charged species of Cu<sub>18</sub>NCs.

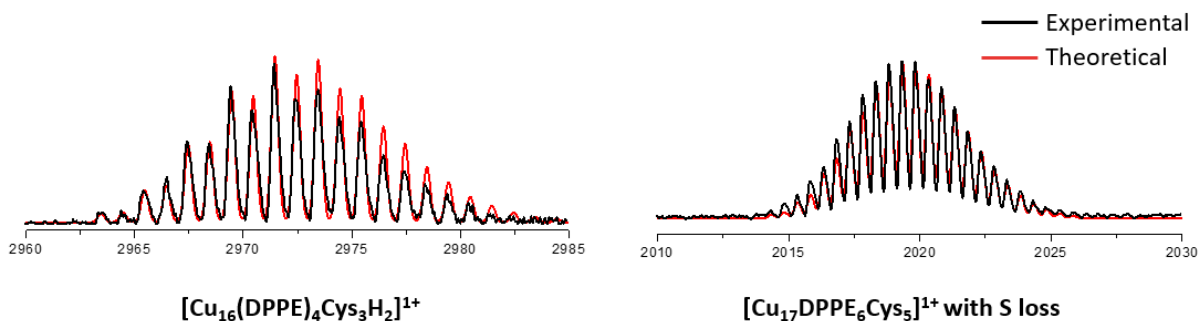


**Figure S2.** Isotopically resolved peaks of the ESI MS features of  $\text{Cu}_{16}\text{NCs}$  (left) and  $\text{Cu}_{17}\text{NCs}$  with one S loss species (right) matched with the theoretical MS spectra.

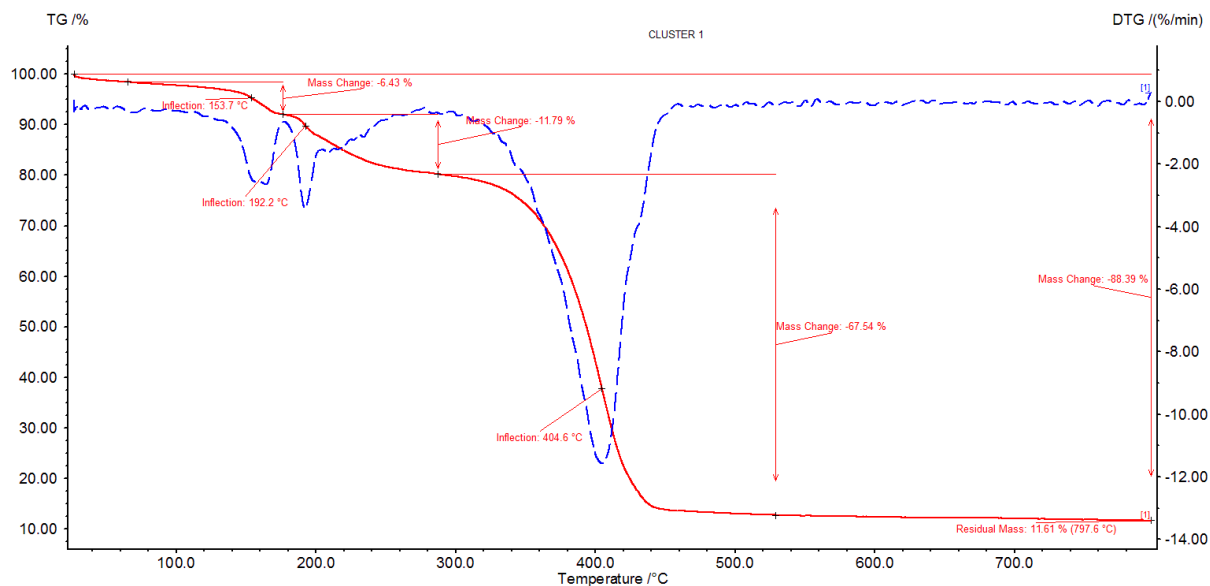


**Figure S3.** TGA and DTA plots of  $\text{Cu}_{17}\text{NCs}$  CASs.

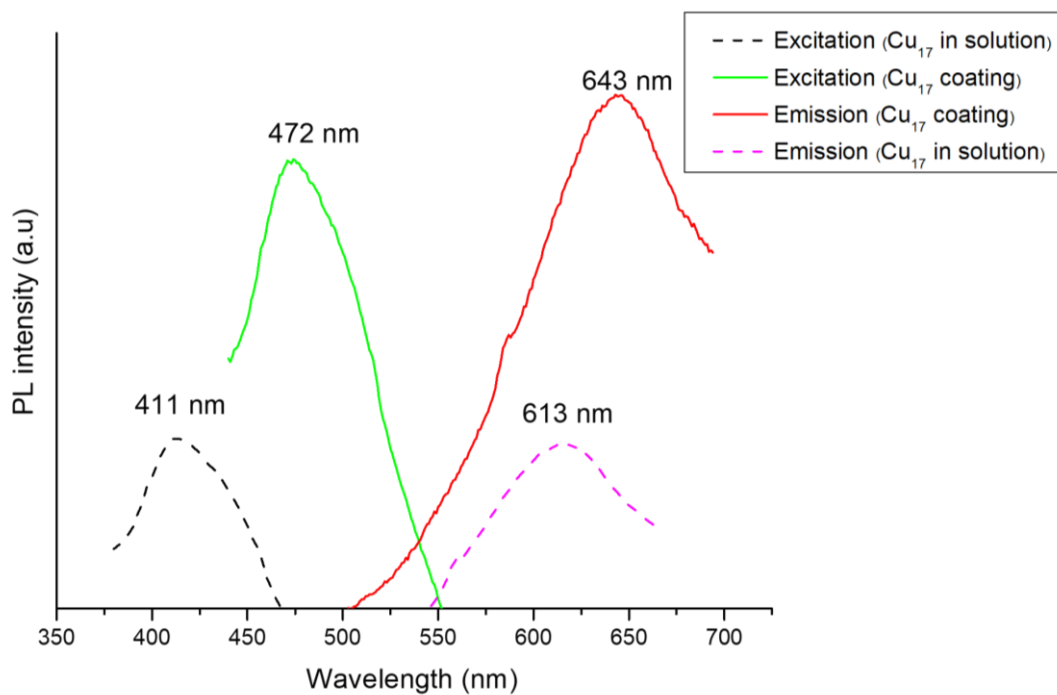


**Figure S4.** PL excitation and emission spectra of  $\text{Cu}_{17}\text{NCs}$  in solution and after the coatings of CASs on PP discs.

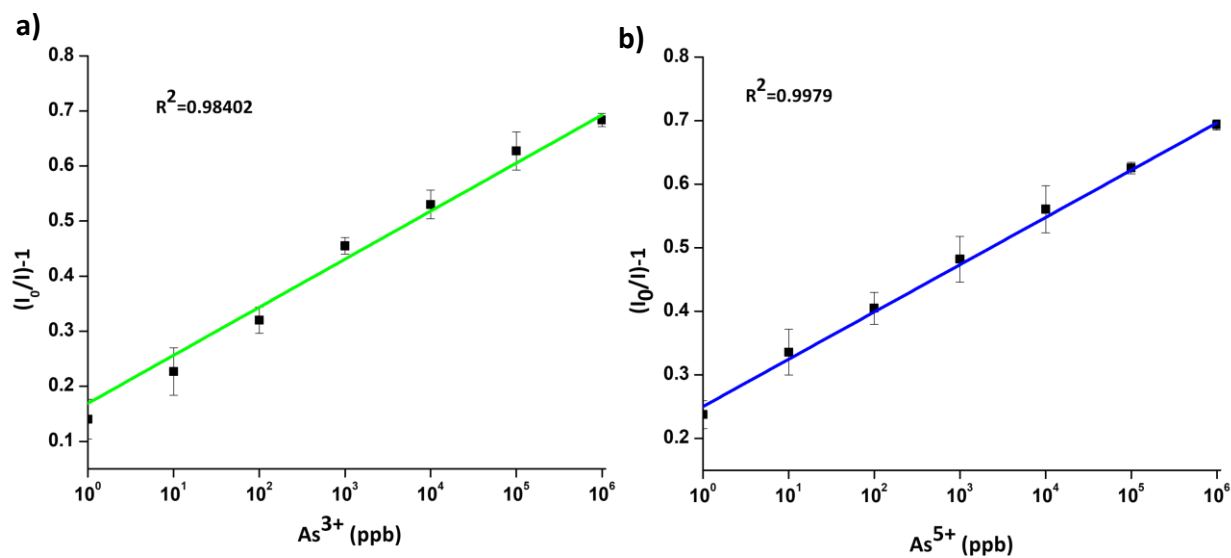


**Figure S5.** Linear regression plots of luminescence sensing with  $\text{Cu}_{17}\text{NCs}$  for a)  $\text{As}^{3+}$  and b)  $\text{As}^{5+}$ .

**Table S1.** Comparison of the salient features of Cu<sub>17</sub>NCs with As sensors reported recently and those available commercially.

Sensor	LOD in ppb	Linear range	Selectivity	Response time	Stability	Cost	Portability & usage	Ref
Cu <sub>17</sub> NCs	1	1-10 <sup>3</sup> ppm	Highly selective to As <sup>3+</sup> and As <sup>5+</sup>	10 min	Stable at room temperature	~\$0.01	Solid state sensor with portability	-
Cobalt NCs	0.66	0-100	Highly selective to As <sup>3+</sup>	~3-5 min	Stable at room temperature	\$1	Electrochemical sensor with liquid buffers	9
Cysteine protected AuNCs	4	-	Highly selective to As <sup>3+</sup>	-	Stable at room temperature	Added cost due to Gold	Liquid phase	10
Electrogenerated Nanotextured Gold Assemblage	0.1	0.1-9	Highly selective to As <sup>3+</sup>	5 min	Stable at room temperature	Costly due to Gold usage	Electrochemistry performed in liquid medium	11
chlorin e6	1.37	0-400 ppm	As <sup>5+</sup> But susceptible to Cu	-	Stable at room temperature Light-sensitive Chlorin e6 used	High due to Chlorin e6 usage	Liquid medium	12
Nanocomposite-modified electrochemical sensor	9	0-2 ppm	Highly selective to As <sup>5+</sup>	>10 min on average	Stable at room temperature	-	Liquid medium employed Preconcentration needed	13
<b>Commercial tests</b>								
HACH, Arsenic test kit, USA	10	0-500	As <sup>3+</sup> and As <sup>5+</sup>	30-35 min	Stable at room temperature	\$1.67	Portable	14
Ascel® Arsenic Test Kit	<10	0-1000	As <sup>3+</sup> and As <sup>5+</sup>	7 min	Stable at room temperature	\$2.99	Portable, Involves generation of arsine gas, the most toxic form of As	15
Arsenator® Digital Arsenic Test Kit, Wagtech WTD, Palintest Ltd, United Kingdom	2	0-100	As <sup>3+</sup> and As <sup>5+</sup>	20 min	Stable at room temperature	\$ 4.59	Portable	16
QUANTOFIX® Arsenic Sensitive Semi-quantitative test strips. MACHEREY-NAGEL GmbH & Co. KG, Düren, Germany, Product No. 91345	5	0-500	As <sup>3+</sup> and As <sup>5+</sup>	10 min	Stable at room temperature	\$ 1.01	Portable	17

Quick™ Arsenic Test Kit, Industrial test systems, Inc., USA Part Number: 481396	5	0–>500	As <sup>3+</sup> and As <sup>5+</sup>	12 min	Stable at room temperature	\$ 1.78	Portable	18
Merckoquant® Arsenic (Merck Germany, Product No. 1.17927.0001)	10	0–500	As <sup>3+</sup> and As <sup>5+</sup>	20 min	Stable at room temperature	\$ 2	Portable	19

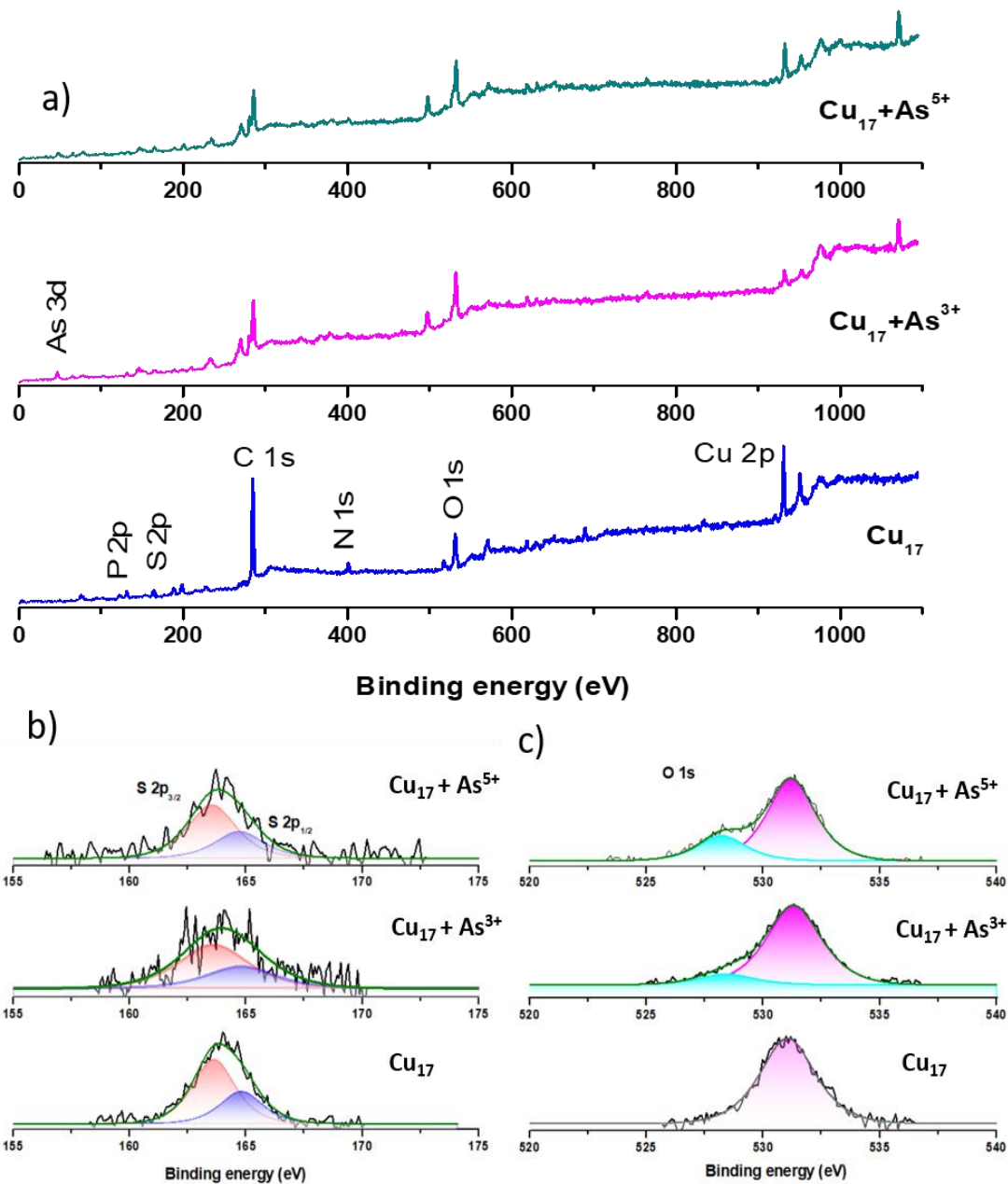


**Figure S6.** a) XPS survey spectra of pure  $\text{Cu}_{17}\text{NCs}$  and that with  $\text{As}^{3+}$  and  $\text{As}^{5+}$ , b) selected XPS spectra in the S 2p and c) O 1s regions.

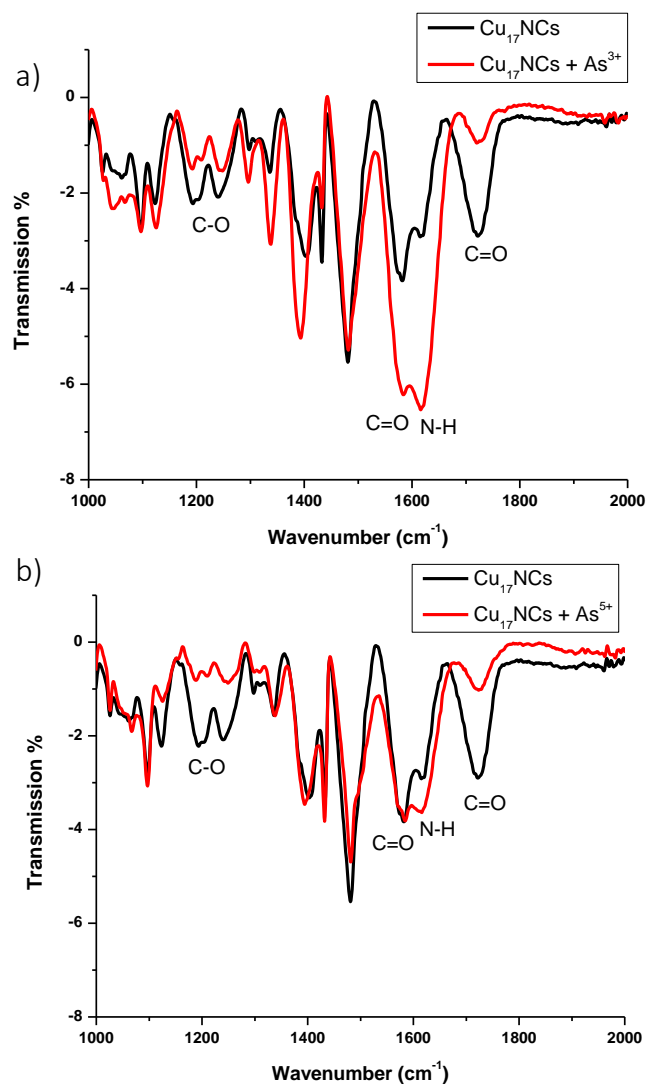


**Figure S7.** FTIR spectra of Cu<sub>17</sub>NCs before and after exposure to a) As<sup>3+</sup> and b) As<sup>5+</sup>.

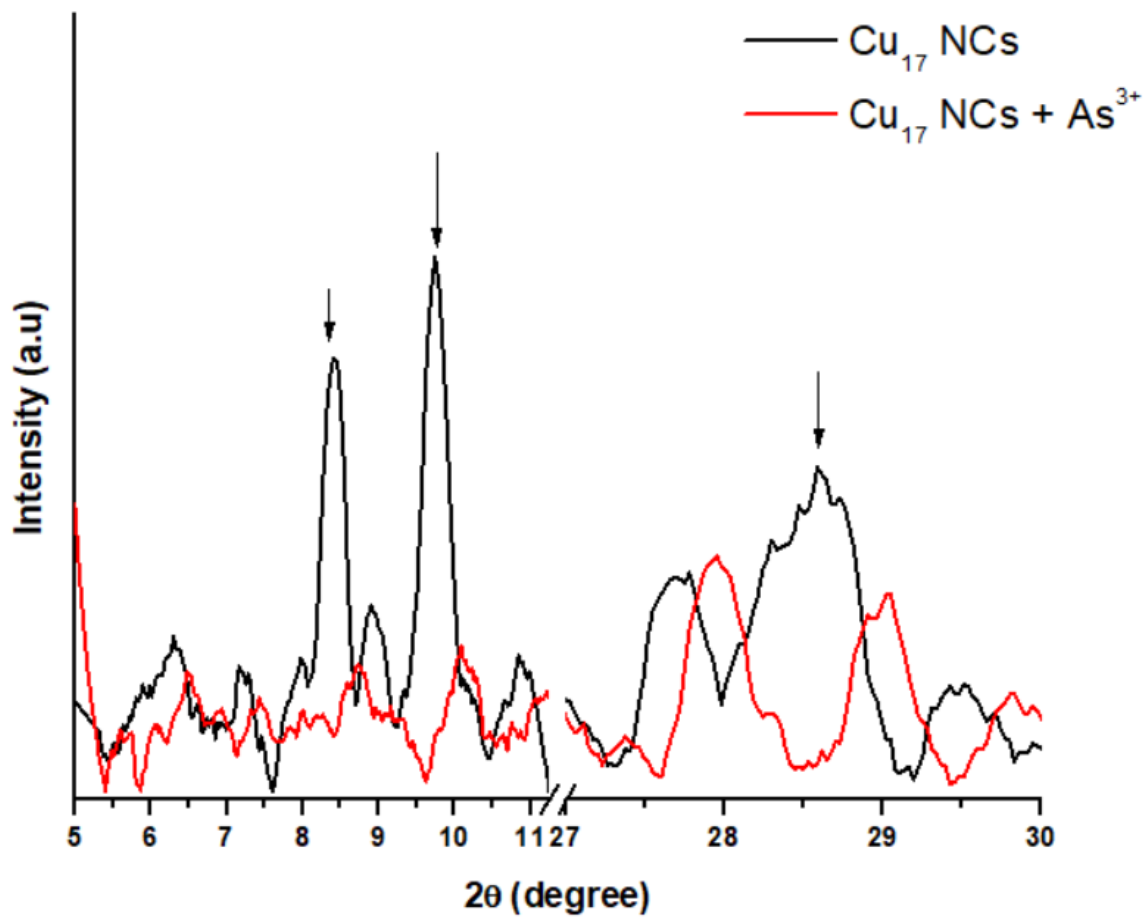


**Figure S8.** Comparative PXRD spectra of Cu<sub>17</sub>NCs and Cu<sub>17</sub>NCs after the exposure to As<sup>3+</sup>.

The arrows indicate the peaks showing significant intensity changes.

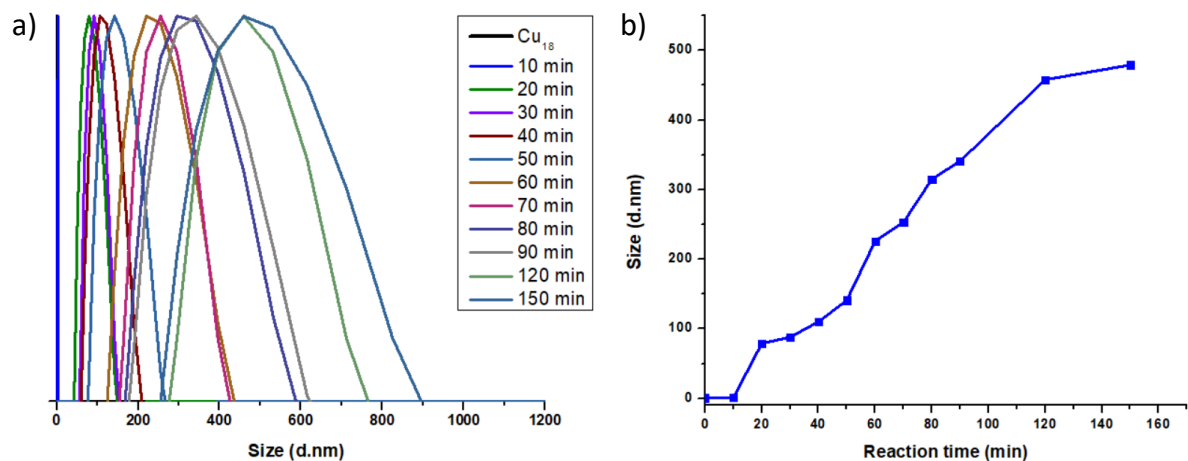


**Figure S9.** a) Time-dependent DLS spectra of the conversion of  $\text{Cu}_{18}\text{NCs}$  into CASs composed of  $\text{Cu}_{17}\text{NCs}$  after adding L-Cys dissolved in methanol. b) Variation of the size of the CASs plotted against time.

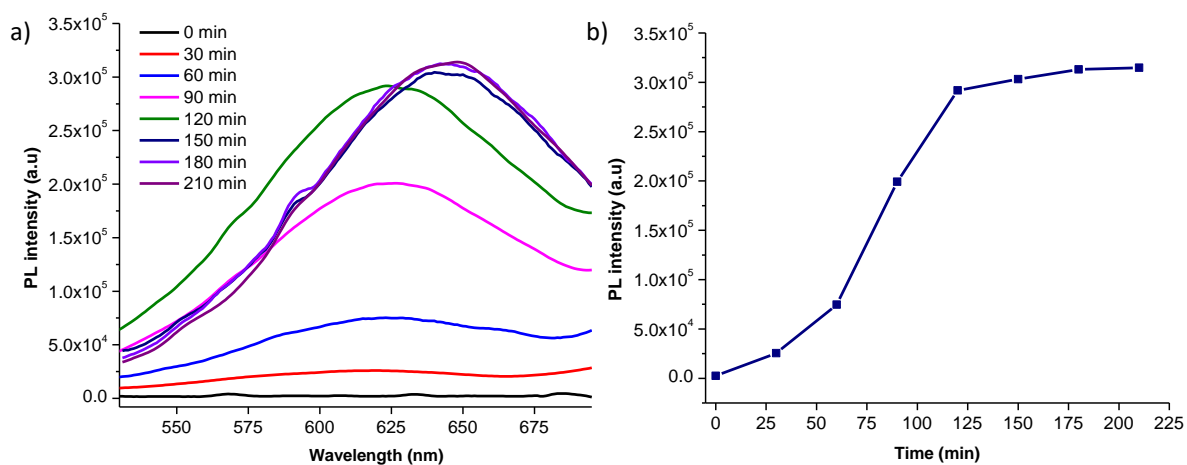


**Figure S10.** a) Time-dependent PL plot of  $\text{Cu}_{17}\text{NCs}$  during synthesis. b) Luminescence intensity vs time plot at 643 nm.

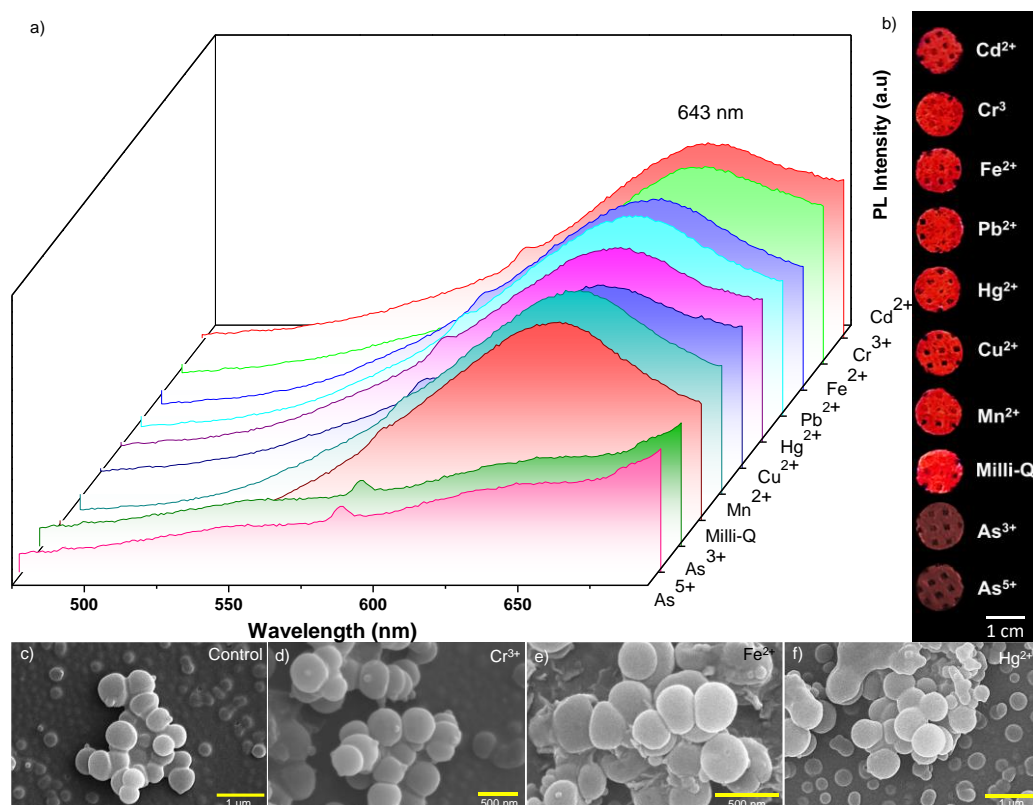


**Figure S11.** a) Comparative PL spectra showing emission quenching by the exposure of  $As^{3+}$  and  $As^{5+}$  ions compared to other water-soluble interfering ions. Excitation was at 472 nm. b) Photographs of CASs sensors under 365 nm UV light show the emission quenching only by  $As^{3+}$  and  $As^{5+}$ . c) FESEM micrographs of CASs and CASs exposed to d)  $Cr^{3+}$ , e)  $Fe^{2+}$  and f)  $Hg^{2+}$  ions. No disruption of the structure was observed for these ions.

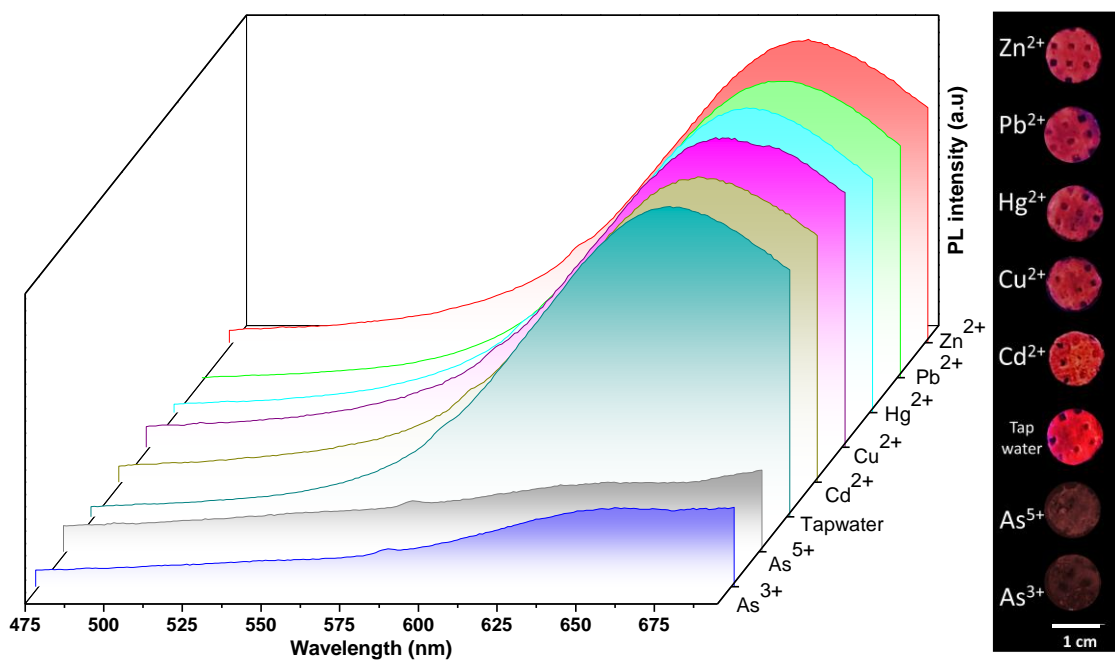


**Figure S12.** Stacked PL spectra of PP discs containing  $\text{Cu}_{17}$  spheroids after exposure to the tap water samples spiked with  $\text{As}^{3+}$ ,  $\text{As}^{5+}$  and interfering ions. Excitation was at 472 nm. The figure on the right shows the photographs (under 365 nm UV light) of the sensing platform after exposure to contaminated tap water.

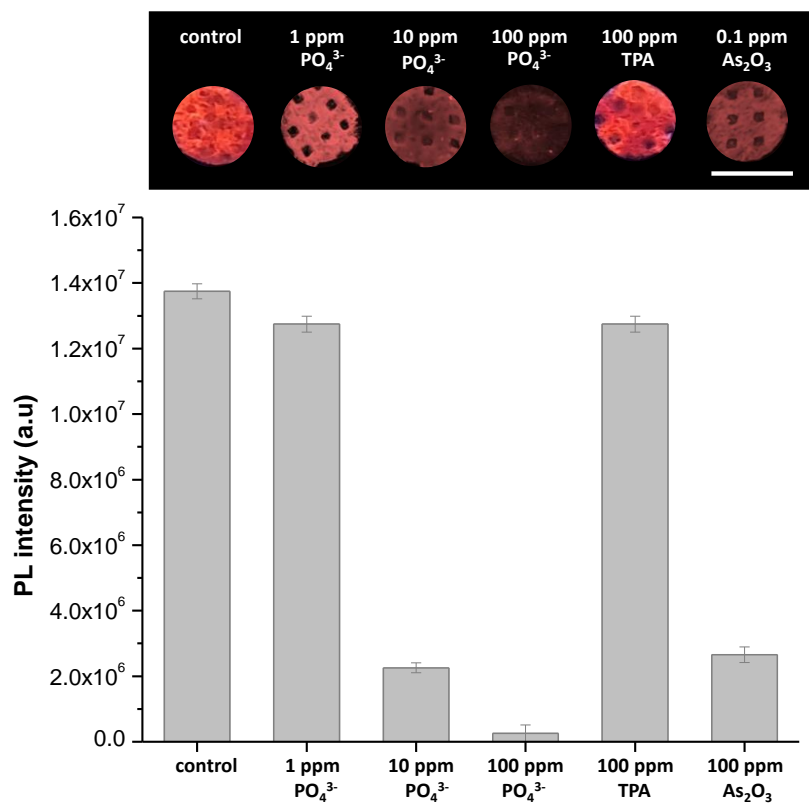


**Figure S13.** Bar graph showing the effect of phosphates ( $\text{PO}_4^{3-}$ ), triphenyl arsine (TPA) and arsenic trioxide ( $\text{As}_2\text{O}_3$ ) on the sensor discs. The inset shows the photographs of the discs under UV light. Phosphate at 10 ppm or higher concentrations can significantly affect the luminescence. 100 ppm of TPA does not affect the emission, while 0.1 ppm of  $\text{As}_2\text{O}_3$  quenches the emission of the NCs. The scale bar is 1 cm.

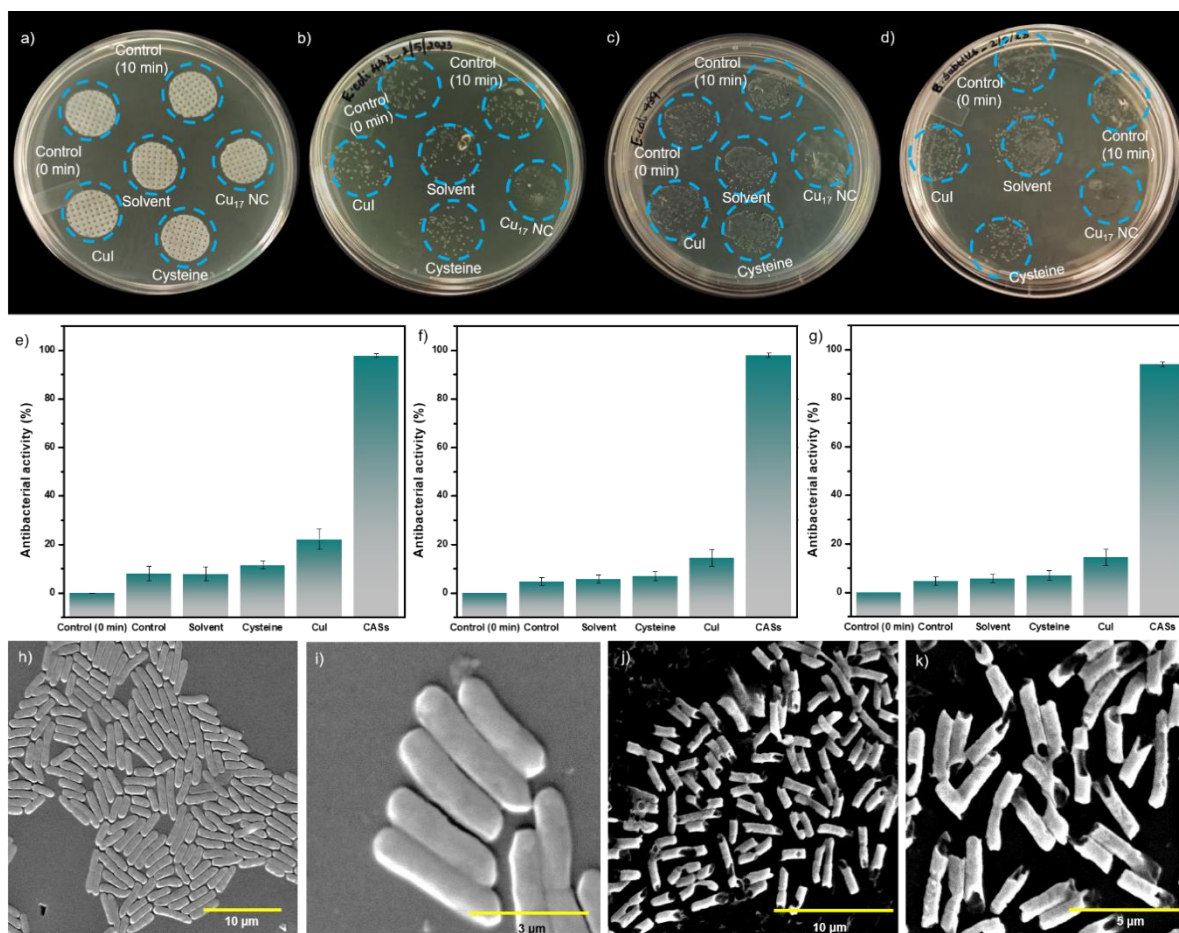


**Figure S14.** Nutrient agar plates showing a) PP discs placed on the plate with bacteria before incubation. Nutrient agar plates incubated at 32 °C for 24 hours show antibacterial activity against b) *E. coli* MTCC 443, c) *E. coli* MTCC 739, and d) *B. subtilis* after 1 h of exposure. Antibacterial activity plots of e) *E. coli* MTCC 443, f) *E. coli* MTCC 739 and g) *B. subtilis*, determined through colony counting method, performed with triplicates. ESEM images of *E. coli* MTCC 443 h) before and j) after the exposure to CASs. i) and k) show the zoomed-in view of the unaffected and affected cell membranes.

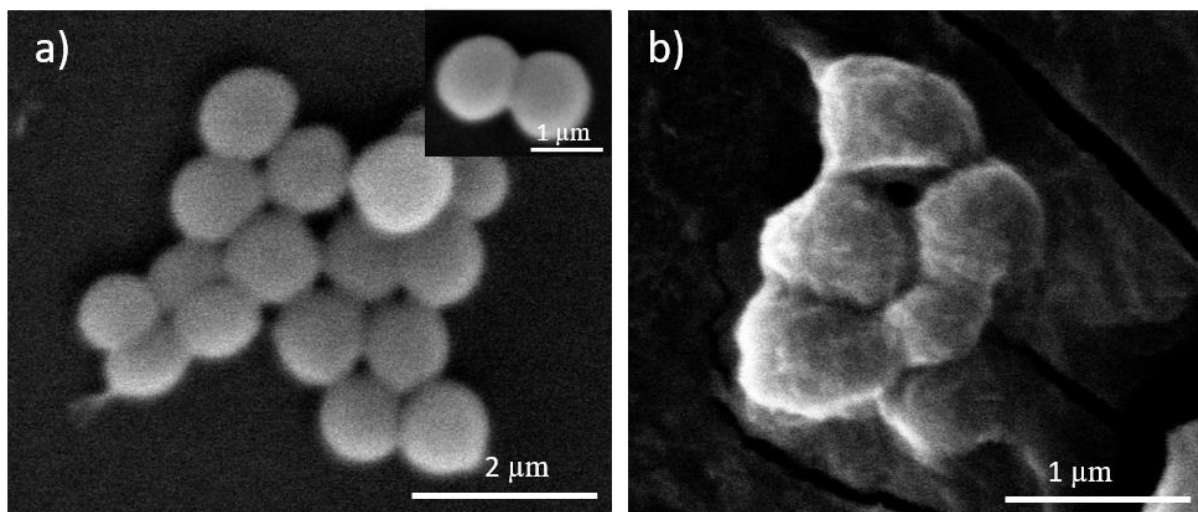


**Figure S15.** Antibacterial activity of CASs against *Staphylococcus aureus*. ESEM images of *S. aureus* a) control and b) cells interacted with CASs (right). Inset of a) shows the control cells in zoomed-in view.

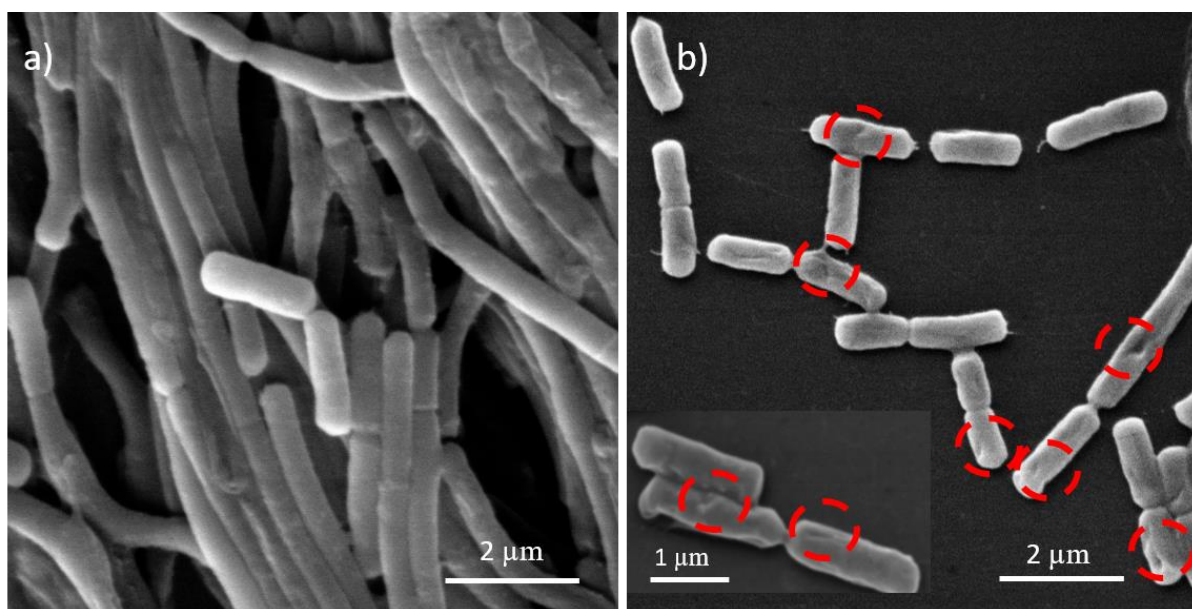


**Figure S16.** Antibiofilm activity of CASs against *B. subtilis*. ESEM images of a) *B. subtilis* control and b) cells interacted with CASs showing cell membrane damage (red dashed circles) (inset shows the zoomed-in view of the damaged cell membrane).

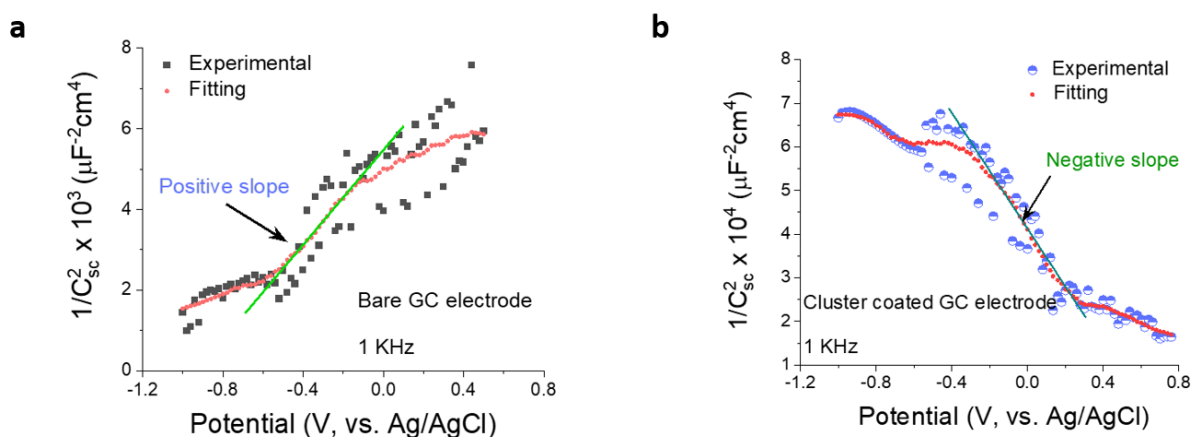


**Figure S17.** Electrochemical impedance spectroscopy measurement of CASs coating. a) The EIS plot of bare GCE and b) Cu<sub>17</sub>NCs coated GCE (right). The experiment was carried out in NaCl.

**Note:**

‡J. Raman and H. M. Veera, from the Department of Biotechnology, Vel Tech High Tech Dr Rangarajan Dr Sakunthala Engineering College, Chennai 600062, India, were having their internships with TP during the course of this work.

**Reference:**

- (1) Li, J.; Ma, H. Z.; Reid, G. E.; Edwards, A. J.; Hong, Y.; White, J. M.; Mulder, R. J.; O’Hair, R. A. J. Synthesis and X-Ray Crystallographic Characterisation of Frustum-Shaped Ligated [Cu<sub>18</sub>H<sub>16</sub>(DPPE)<sub>6</sub>]<sup>2+</sup> and [Cu<sub>16</sub>H<sub>14</sub>(DPPA)<sub>6</sub>]<sup>2+</sup> Nanoclusters and Studies on Their H<sub>2</sub> Evolution Reactions. *Chem. – A Eur. J.* **2018**, *24* (9), 2070–2074. <https://doi.org/10.1002/chem.201705448>.
- (2) Jia, X.; Li, J.; Wang, E. Cu Nanoclusters with Aggregation Induced Emission Enhancement. *Small* **2013**, *9* (22), 3873–3879. <https://doi.org/10.1002/sml.201300896>.
- (3) Farrag, M.; Das, M. K.; Moody, M.; Samy El-Shall, M. Ligand-Protected Ultrasmall

- Pd Nanoclusters Supported on Metal Oxide Surfaces for CO Oxidation: Does the Ligand Activate or Passivate the Pd Nanocatalyst? *ChemPhysChem* **2021**, *22* (3), 312–322. <https://doi.org/10.1002/cphc.202000656>.
- (4) Jana, A.; Jash, M.; Dar, W. A.; Roy, J.; Chakraborty, P.; Paramasivam, G.; Lebedkin, S.; Kirakci, K.; Manna, S.; Antharjanam, S.; Machacek, J.; Kucerakova, M.; Ghosh, S.; Lang, K.; Kappes, M. M.; Base, T.; Pradeep, T. Carborane-Thiol Protected Copper Nanoclusters: Stimuli-Responsive Materials with Tunable Phosphorescence. *Chem. Sci.* **2023**, *14* (6), 1613–1626. <https://doi.org/10.1039/D2SC06578A>.
- (5) Jeong, Y.; Yoon, J. Recent Progress on Fluorescent Chemosensors for Metal Ions. *Inorganica Chim. Acta* **2012**, *381*, 2–14. <https://doi.org/10.1016/j.ica.2011.09.011>.
- (6) Baghdasaryan, A.; Bürgi, T. Copper Nanoclusters: Designed Synthesis, Structural Diversity, and Multiplatform Applications. *Nanoscale* **2021**, *13* (13), 6283–6340. <https://doi.org/10.1039/D0NR08489A>.
- (7) Sahu, B.; Kurrey, R.; Deb, M. K.; Shrivastava, K.; Karbhal, I.; Khalkho, B. R. A Simple and Cost-Effective Paper-Based and Colorimetric Dual-Mode Detection of Arsenic(III) and Lead(II) Based on Glucose-Functionalized Gold Nanoparticles. *RSC Adv.* **2021**, *11* (34), 20769–20780. <https://doi.org/10.1039/D1RA02929K>.
- (8) Yuan, X.; Zhu, M. Recent Advances in Atomically Precise Metal Nanoclusters for Electrocatalytic Applications. *Inorg. Chem. Front.* **2023**, *10* (14), 3995–4007. <https://doi.org/10.1039/D3QI00656E>.
- (9) Jose, A.; Jana, A.; Gupte, T.; Nair, A. S.; Unni, K.; Nagar, A.; Kini, A. R.; Spoorthi, B. K.; Jana, S. K.; Pathak, B.; Pradeep, T. Vertically Aligned Nanoplates of Atomically Precise Co<sub>6</sub>S<sub>8</sub> Cluster for Practical Arsenic Sensing. *ACS Mater. Lett.* **2023**, *5* (3), 893–899. <https://doi.org/10.1021/acsmaterialslett.3c00085>.

- (10) Roy, S.; Palui, G.; Banerjee, A. The As-Prepared Gold Cluster-Based Fluorescent Sensor for the Selective Detection of As<sup>III</sup> Ions in Aqueous Solution. *Nanoscale* **2012**, *4* (8), 2734–2740. <https://doi.org/10.1039/C2NR11786J>.
- (11) Babar, N. U. A.; Joya, K. S.; Tayyab, M. A.; Ashiq, M. N.; Sohail, M. Highly Sensitive and Selective Detection of Arsenic Using Electrogenerated Nanotextured Gold Assemblage. *ACS Omega* **2019**, *4* (9), 13645–13657. <https://doi.org/10.1021/acsomega.9b00807>.
- (12) Luo, M.-L.; Chen, G.-Y.; Wang, J.-L.; Chai, T.-Q.; Qian, Z.-M.; Li, W.-J.; Yang, F.-Q. Detection of Arsenic(V) by Fluorescence Sensing Based on Chlorin E6-Copper Ion. *Molecules*. 2024. <https://doi.org/10.3390/molecules29051015>.
- (13) Hamid Kargari, S.; Ahour, F.; Mahmoudian, M. An Electrochemical Sensor for the Detection of Arsenic Using Nanocomposite-Modified Electrode. *Sci. Rep.* **2023**, *13* (1), 8816. <https://doi.org/10.1038/s41598-023-36103-6>.
- (14) HACH Low Range Arsenic Test Kit <https://www.hach.com/p-arsenic-low-range-test-kit/2800000>.
- (15) Ascel® Arsenic Test Kit - 50-Tests <https://sensafe.com/ascel-arsenic-50-tests/>.
- (16) Digital Arsenic Test Kit <https://www.palintest.com/products/arsenator/>.
- (17) Semi-quantitative test strips QUANTOFIX EZ Arsenic Sensitive PP <https://www.mn-net.com/semi-quantitative-test-strips-quantofix-ez-arsenic-sensitive-pp-91345.2>.
- (18) Quick™ Arsenic for Water, Soil, and Wood Test Kit <https://sensafe.com/481396/>.
- (19) MQuant® Arsenic Test [https://www.merckmillipore.com/IN/en/product/Arsenic-Test,MDA\\_CHEM-117927](https://www.merckmillipore.com/IN/en/product/Arsenic-Test,MDA_CHEM-117927).

